ELSEVIER

Journal of Nuclear Materials 313–316 (2003) 914–918

journal of nuclear materials

www.elsevier.com/locate/jnucmat

Patterns of ELM impacts on the JET wall components

Ph. Ghendrih [a,*], Y. Sarazin [a], M. Bécoulet [a], G. Huysmans [a], S. Benkadda [b], P. Beyer [b], C. Figarella [b], X. Garbet [a], P. Monier-Garbet [a], JET team

[a] *Association Euratom-CEA, DRFC/DSM/CEA, CEA Cadarache, F-13108 St. Paul lez Durance, cedex, France*
[b] *PIIM, Université de Provence, 13397 Marseille, cedex 20, France*

Received 27 May 2002; accepted 12 September 2002

Abstract

Numerical analysis of the images in visible light from the JET tangential camera show that the edge localised mode (ELM) events are characterised by impacts on the low-field side components. The increase of emission is not restricted to the components closest to the plasma. One finds also that the deposition on the low-field side components does not exhibit any poloidal or toroidal symmetry and varies from ELM to ELM. Conversely the increase of emission on the divertor baffles, or the top protection tiles, is close to axisymmetric.
© 2003 Elsevier Science B.V. All rights reserved.

PACS: 52.25.Fi; 52.35.Ra; 52.40.Hf; 52.30.Jb
Keywords: ELM; Local deposition; Wall components; JET; Avalanche transport; Visible light emission

1. Introduction

Present fusion experiments have provided a comprehensive description of the main reference scenario selected for ITER, namely the edge localised mode (ELM)y H-mode [1]. However, bringing together the constraints of high core performance and that of a viable divertor operation is not fully resolved yet. In particular, the ELMs lead to very high energy loads to the target plates that might severely reduce the life time of those components [2].

To date, there is no empirical or theoretical approach that provides a convincing extrapolation of ELM characteristics from that met on present devices to those that will be met on ITER [3]. Part of the difficulty could be linked to the wide range of ELM behaviours that exist, type I, II and type III ELMs, the compounds ELMs, mixed ELM regimes, as well as other patterns such as possible unstable periodic orbits [4].

The aim of the paper is to investigate means of improving the description of ELMs. The visible light emission recorded by the tangential camera of JET is analysed. Clear evidence of localised interaction with the first wall of the main chamber is reported.

2. ELM impact in the main chamber of JET

The analysis of the visible light emission presented here is restricted to JET shots obtained during an experimental session dedicated to increasing the H-mode natural density (with no gas injection). The shots have standard shaping $\Delta \sim 0.23$ with the Mark II GB divertor (with septum). Routine magnetic field, 2.5 T, and plasma current, 2.5 MA are used. The level of beam heating is moderate, $P_{\text{total}} \sim 12$ MW. For these conditions, the H-mode density rapidly rises to a Greenwald fraction of $f_G \sim 0.7$ so that the H-mode threshold power P_{LH} increases and reaches half of the input power P_{total}. When this condition is achieved the density appears to level-off as the discharge parameters approach the boundary between the type-I ELMy H-mode with good energy and particle confinement time and type III ELMy

* Corresponding author. Tel.: +33-4 4225 2993; fax: +33-4 4225 4990.
E-mail address: ghendrih@drfc.cad.cea.fr (Ph. Ghendrih).

0022-3115/03/$ - see front matter © 2003 Elsevier Science B.V. All rights reserved.
PII: S0022-3115(02)01476-9

H-mode with confinement properties nearly degraded down to that of the L-mode [5].

The tangential camera of JET records visible light emission from a large fraction of the JET vessel. Its characteristic time is rather slow, 40 ms per frame. This time is governed by the sweep time of the camera, but does correspond to a 40 ms averaging process of the emission. The videotape of a series of shots has been digitised and numerical treatment is used to extract relevant data regarding the ELM behaviour.

The camera collects all visible light emission, hence both recycling deuterium and light impurities. The local emission is thus related to the recycling pattern with an indirect link to the energy deposition pattern (use of such a relationship will also be found in Ref. [6]).

The Fourier transform in time of the images of the tangential camera has proven to be a powerful tool to analyse Tore Supra long pulse operation [7]. However, in the case of ELMy discharges, the Dirac like ELM peaks lead to a 'white noise' Fourier transform that is difficult to interpret. A more direct treatment has been used here. It is based on image averaging using different filters. In a first step, a reference signal is chosen and sampled at the rate of the tangential camera. In this paper, the time trace of the emission from one point of the frame has been used, Fig. 1. A threshold is then defined that discriminates the ELM events, such that the magnitude of the signal is larger than the threshold, from the 'non-ELM' events, such that the magnitude of the signal is smaller than the threshold. Two filtering signals are then readily built as a sequence of 1 and 0 depending of the relative magnitude of the emission with respect to the threshold. The ELM filter has its 'ones' at the ELM occurrence time and the non-ELM filter has its 'ones' when it does not coincide to an ELM occurrence time. These signals are then used to determine the average image during an ELM and during a non-ELM. The difference between these two images provides the image of the change in visible light emission that takes place during the ELMs, Fig. 2. The outstanding features of this emission pattern are a reduced emission from the high-field components and an enhanced emission from the divertor baffles as well as from the high-field scrape-off-layer (SOL) extending from the midplane to the divertor baffle. On the low-field, enhanced emission is observed on several components, mostly the guard limiters of the ICRH antennas, Fig. 2, the closest elements to the plasma. The gap between the plasma and the

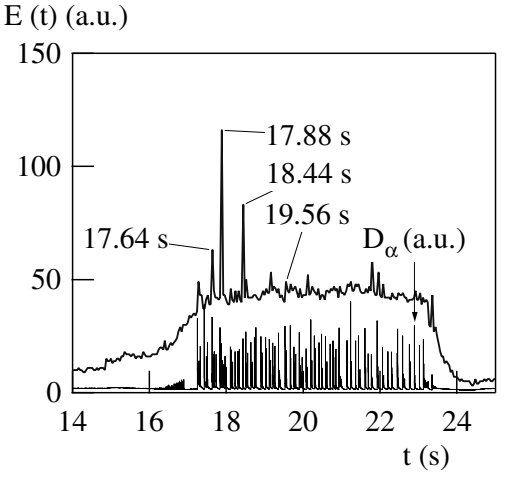

Fig. 1. Time trace of the emission of visible light. The emission saturates at a value of 256. Spikes are associated to ELMs. The rise of the background emission corresponds to the H-mode phase of the discharge. The various times highlighted on the plot correspond to the time used in Figs. 3 and 4 to draw the emission profiles. The trace of the D_α emission is also displayed (with different units).

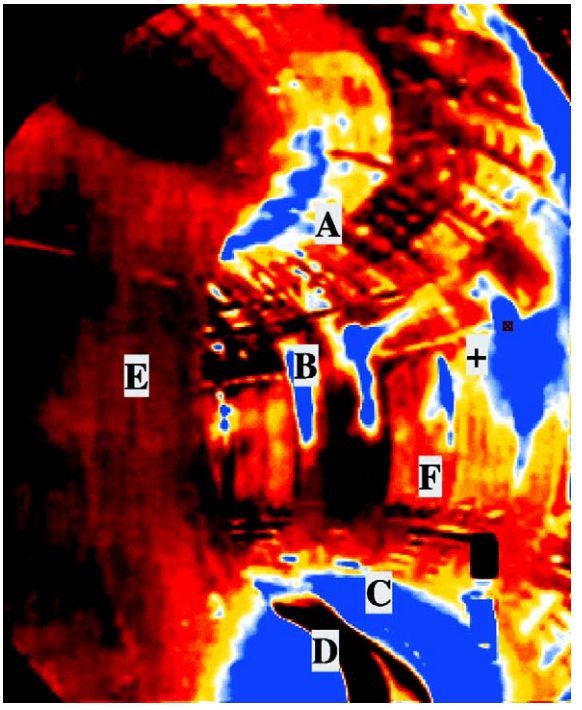

Fig. 2. Image of the visible light emission in JET after filtering. This image is the difference between the average of the emission during the ELMs and the average of the emission when no ELM is detected. The intensity is in arbitrary units and the colour ordering is the following, black, red, yellow, white blue, black being 'cold' and blue 'hot'. The 'cold' regions are those where the visible emission has decreased or weakly changed. The 'hot' regions correspond to significant emission increase during the ELMs. In this treatment contrast is enhanced. Lettering on the figure locates the various components, A the top protection tiles, B one of the ICRH guard limiters, C outboard baffle and low field-side SOL, D inboard baffle, E inner wall, F ICRH antenna. The point identified by the plus sign '+' is that used in Fig. 1 to plot the time trace of the emission.

guard limiters is 0.07 m at the top and midplane locations and reaches 0.14 m at the lowest location. Impact of ELMs on the ICRH limiters has already been reported [8]. However, the present data indicates that ELM impacts are also seen on more distant components such as the ICRH antennas themselves (recessed a couple of centimetres further back). The unbalance of the emission pattern between the low- and high-field parts of the main chamber agrees with the predicted location of the linearly unstable modes, both ballooning and pealing modes [9]. It also agrees with the ELM outflow to the low-field side only, as observed in double null configurations of DIII-D [10]. The interaction of the ELM with distant objects in the low-field side SOL has also been reported in DIII-D [11] or MAST [12]. While cross-field transport exhibits the ballooning localisation, one finds an increase of recycling on the divertor baffles, both on the low-field and on the high-field side. Parallel transport both co- and counter the magnetic field, which competes with the cross-field transport on the open field lines, will tend to generate a more symmetric deposition pattern.

The image obtained by the filtering technique provides the average ELM behaviour but does not yield the impact per ELM. In the following, we display profiles of the emission along various lines. One can then analyse the emission profiles, $E_t(s)$ where t is the time and s is the curvilinear abscissa. For the profiles that are presented here, one considers the change of emission at each ELM, $\Delta E_t(s) = E_t(s) - E_{t-\delta t}(s)$. The time t is then the occurrence time of an ELM (using the same definition as in the filtering procedure), and $t - \delta t$ the time of the previous frame, $\delta t = 0.04$ s being the sampling rate.

Let us first consider the emission along a given line to investigate the poloidal symmetry. The line starts at the top of the machine on the protection tiles, $s \leqslant 52$, and follows the intersection of a poloidal plane and the wall of the main chamber. It thus follows the outboard vessel contour, passing over various wall components before reaching the ICRH antenna, from $s \geqslant 106$ to $s \leqslant 179$. It then extends over the outboard baffle, $s \geqslant 224$, and finally the divertor. Three main regions of emission change ΔE_t can be seen (Fig. 3) the divertor baffle, the ICRH antenna and the top tiles. The divertor region itself is characterised by a small change of emission. The divertor emission does not appear to increase much during the ELMs, hence $\Delta E \sim 0$. The emission from the baffle and the region between the baffle and the ICRH antenna changes from ELM to ELM, Fig. 3. The maximum, localised in the baffle region, close to the divertor, does not vary significantly from ELM to ELM. Conversely, the extent towards the ICRH antenna is rather sensitive. For a small ELM event at $t = 19.56$ s, the change in emission is well localised to the baffle region, $\Delta s \sim 20$. For the larger ELM events, the change in emission extends to $\Delta s \sim 30$ at $t = 18.44$ s and $\Delta s \sim 50$

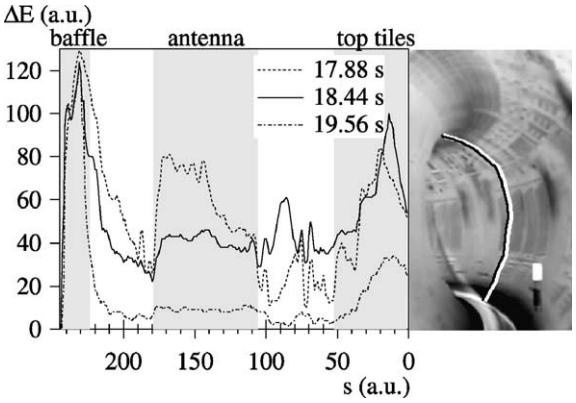

Fig. 3. Emission profile from a poloidal line running from the divertor to the top protection tiles at the intersection of a poloidal plane and the outer wall. Strong emission regions are highlighted by the shaded areas, baffle, ICRH antenna and top tiles. The three selected times correspond to emission peaks (see Fig. 1).

at $t = 17.88$ s. The emission from the ICRH antenna exhibits a similar trend. It is very large at $t = 17.88$ s, with a specific up-down asymmetry, still large at $t = 18.44$ s with a maximum in the middle, and much weaker for the smaller ELM at $t = 19.56$ s. At $s \sim 85$, there is a peak for the $t = 18.44$ s ELM. It is the trace of a radiation plume, originating from an ICRH guard limiter and extending toroidally. It provides a 'measure' of the poloidal extent of the ELM impact, $\Delta s \sim 20$. This extent is similar to that of the maximum observed on the ICRH antenna for the same ELM event at a distance $\delta s \sim 55$. Provided one can relate the distance from the top tile peaks to the divertor baffle peaks ($\delta s \sim 216$) to a poloidal angle of π, then the main poloidal mode number of this deposition pattern would be fitted by a simulation of linear ballooning modes with $n = 12$ and $m \sim 50$ [13]. However, unlike the simulation output, the observed peaks on the guard limiters have very different magnitudes in agreement with the overall result that there is no poloidal symmetry in the ELM emission.

For a line drawn by following the helical pattern of emission (including the radiation plume discussed above), Fig. 2, one can observe ELM impacts on the guard limiters, but with a distribution in magnitude that varies from limiter to limiter, Fig. 4. One can notice that the increase of emission also occurs in regions where components are recessed behind the limiters. Finally as reported for the poloidal line, the emission pattern changes from ELM to ELM. This indicates that there is no toroidal symmetry in the ELM deposition on the low-field side components. Although the emission appears to extend along the field line in the vicinity of the ELM impact (radiation plume), there is no marked feature of a flute like emission (with $k_{\|} = 0$).

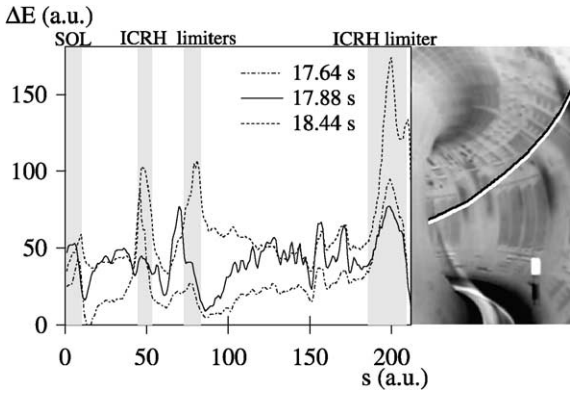

Fig. 4. Emission profile from a line following a rotational transform on the low-field side of the vessel. Strong emission regions are highlighted by the shaded areas, high-field SOL, and three ICRH guard limiters. The three selected times correspond to emission peaks (see Fig. 1).

When analysing the radiation from the baffle region, one finds a near axisymmetric radiation pattern. The toroidal variation is less than 30%. In the poloidal direction, one finds that the radiation appears to extend out of the divertor volume at each ELM. The emission in the divertor itself decreases slightly, but extends poloidally over the septum and to the baffles (high- and low-field). One finds that the emission is rather flat throughout this region, hence from the inboard baffle to the outboard baffle. The divertor appears to be plugged during the large ELM events, namely that the parallel transport into the divertor, and subsequently the control it provides, is inefficient, or at least does not appear to be different from the parallel transport onto the baffles. The decay rate away from the baffles changes from ELM to ELM. When analysing the non-ELM radiation from the high-field SOL, one finds that the emission peaks at the separatrix and decays in the near SOL before flattening out to the wall. During the ELM events, the emission is slightly reversed, peaking at the wall and decaying to the separatrix. Superimposed to this structure, one can observe various emission peaks that might be interpreted as the signature of heat flux channels with varying radial locations.

3. Discussion and conclusion

The various signatures of the ELM activity reported here, in particular the localised ELM impact on the low-field side of the JET chamber, are reminiscent of the localised cross-field transport reported in turbulence simulations and associated to avalanche or front propagation phenomena [14]. Interestingly, these turbulence models, when driven to generate a transport barrier, exhibit relaxation modes, called Barrier Relaxation Modes, that bare many common features with the ELMs [15].

A striking feature of the analysis of the images of the tangential camera is the poor relationship with the ELM activity monitored by the D_α signal, Fig. 1. In the region viewed by the camera, less than 10 ELMs are clearly visible. Those ELMs are associated to ELM impact on the low-field side components. For these events, emission from the high-field side is roughly constant. This confirms the ballooning structure of ELM transport. Furthermore the present analysis indicates that the ELM impact on the low-field side components is localised both poloidally and toroidally. In some cases, one can observe poloidally 2 or 3 regions of enhanced emission. The geometry of these peaks would fit a linear ballooning calculation with $n = 12$ and $m \sim 50$. Regarding the top tiles and the divertor emission, one finds a far more axisymmetric pattern. As the ELM collapses through the region of strong magnetic shear it will provide a source term for parallel transport to the wall components (both co- and counter the magnetic field). The shearing acting on this parallel transport will generate a fanning effect that could lead to the observed reduction in peaking of the emission on these components.

Analysis of the images of the tangential camera provides important information on the interaction of the ELMs with the main chamber. Further analysis is required to determine the parameters that control the ELM impacts.

Acknowledgements

The authors are most indebted to C. Desgranges and P. Messina for processing the CCD data.

References

[1] G. Janeschitz, J. Nucl. Mater. 290–293 (2001) 1.
[2] G. Federci, J.N. Brooks, D.P. Coster, G. Janeschitz, A. Kukushkin, et al., J. Nucl. Mater. 290–293 (2001) 260.
[3] A. Loarte, these Proceedings.
[4] A.W. Degeling, Y.R. Martin, P.E. Bak, J.B. Lister, X. Llobet, Plasma Phys. Control. Fusion 43 (2001) 1671.
[5] R. Sartori, D. Borba, R. Budny, G.D. Conway, J.G. Cordey et al., Proceedings of the 26th EPS on Plasma Phys. Control. Fusion, Maastricht, 1999, P1.022, p. 42.
[6] Mitteau et al., these Proceedings.
[7] P. Ghendrih, M. Bécoulet, L. Costanzo, Y. Corre, C. Grisolia, et al., Nucl. Fusion 41 (2001) 1401.
[8] R.D. Gill, B. Alper, S. Arshad, A.D. Cheetham, N. Deliyanakis, et al., Nucl. Fusion 39 (1998) 1461.
[9] G.T.A. Huysmans, S.E. Sharapov, A.B. Mikhailovskii, W. Kerner, Phys. Plasmas 8 (2001) 4292.

[10] C.J. Lasnier, A.W. Leonard, T.W. Petrie, J.G. Watkins, J. Nucl. Mater. 290–293 (2001) 1093.
[11] D.L. Rudakov, J.A. Boedo, R.A. Moyer, S. Krasheninnikov, A.W. Leonard, et al., Plasma Phys. Control. Fusion 44 (2002) 717.
[12] G. Counsell et al., these Proceedings.
[13] G. Huysmans, private communication.
[14] Y. Sarazin et al., these Proceedings.
[15] Y. Sarazin, P. Beyer, private communication.